Supercapacitors

18

Narendra Kurra [1,2] and Qiu Jiang [3]
[1]School of Chemistry, Indian Institute of Science Education and Research Thiruvananthapuram (IISER-TVM), Thiruvananthapuram, Kerala, India; [2]Department of Chemistry, Indian Institute of Technology Hyderabad, Kandi, Sangareddy, Telangana, India; [3]School of Materials and Energy, University of Electronic Science and Technology of China, Chengdu, PR China

1. Introduction

The rapid depletion of fossil fuels with adverse environmental impacts led to the deployment of pollution-free renewable energy resources. Though renewables such as solar, wind, and thermal do provide infinite energy, their intermittency poses a major concern. In this scenario, efficient electrochemical energy storage technologies offer sustainable solution toward development of fossil fuel−free society. For instance, lithium-ion batteries offer high energy density up to 270 Wh/kg, but often suffer from poor power density and cycle life. Sluggish mass diffusion kinetics of ions across the electrode material with subsequent volume expansion/contraction during charge/discharge cycles make batteries operate slowly for a limited number of cycles. Alternatively, dielectric capacitors store charge electrostatically and can be operated in milliseconds time scales but at a limited energy density of 10^{-2} Wh/kg. Though supercapacitor is a trade name for commercial electrical double-layer capacitor, it is being used in literature to refer to EDLCs or electrochemical capacitors (ECs). At operating time scales of a few seconds, supercapacitors do store more energy than batteries, and they can last longer than batteries. High efficiency, reversible storage of charges for millions of cycles at fast charge-discharge rates make supercapacitors potential power devices for many applications. A few applications with low energy requirements (5−10 Wh/kg), supercapacitors may even replace batteries. Batteries can also be operated in high power mode without losing their cycling stability by operating them in tandem with supercapacitors [1].

Electrochemical energy storage (EES) technologies offer optimal gravimetric (volumetric) energy/power performance metrics in comparison to other storage technologies including pumped hydro, mechanical, thermal, and magnetic. Moreover, ease of integration with renewable sources that are intermittent in supply of energy, EES offers an advantage in constant supply of energy at demand. Supercapacitors do not need constant voltage for charging unlike batteries, and as a result open up opportunities for the development of self-powered autonomous energy storage devices. For instance, regenerative braking energy has been exploited in charging supercapacitors.

The amount of charge that can be stored and delivered from an energy storage device is primarily dependent on the nature of charge storage mechanism of electrode materials, architecture, and device configuration. The shift from double-layer charging in porous carbon materials to redox charging in transition metal compounds is to bridge the gap between supercapacitors and batteries with the aim of achieving simultaneous high-energy at high-power performance.

2. Basics of charge storage

2.1 Electric charge

An electric charge can be generated by rubbing two objects against each other; this is the well-known triboelectric effect. Thales of Miletus rubbed amber with a cloth which caused attraction of lightweight particles, the basis for discovery of electric charges. Significant experimental efforts led by Michael Faraday, Thomson, and Millikan on the nature of electron provided pathways for the molecular electronic level understanding of electricity [2].

Fundamentally, attraction and repulsion are two main characteristics of charges; repulsive forces operate between like charges and attractive forces operate between opposite charges. The smallest unit of "free" charge is considered to be the charge on an electron or a proton that has a magnitude of

$$e = 1.602 \times 10^{-19} C \tag{18.1}$$

Quantized unit of a negative charge $(-e)$ is carried by an electron while proton is designated to carry one unit of positive charge $(+e)$.

After initial understanding about the nature of electric charge, development of Leyden jar has led to the new phenomenon of charge separation and storage. On the two surfaces of the Leyden jar two metal foils are separated by a layer of glass (Fig. 18.1). Thus, such capacitor separates and stores charges in an electrostatic manner, considered as a basis for the further developments in capacitor technologies over centuries.

2.2 Energy storage in a capacitor

A capacitor is often described as a passive circuit element in an electronic circuitry. It consists of two metallic conductors that are separated by a dielectric material. On application of a potential difference across the conducting plates, an electric field drives accumulation of positive Q^+ and negative charges Q^- on the plates, which are physically separated by a dielectric layer. Thus, transient charge storage is possible in the form of electrostatic field between conducting plates. Ideally, there is no current flow across the capacitor during the charging process.

The linear relationship between amount of charge stored (Q) in a capacitor and electric potential difference between the plates (V) is given by

$$Q = CV \tag{18.2}$$
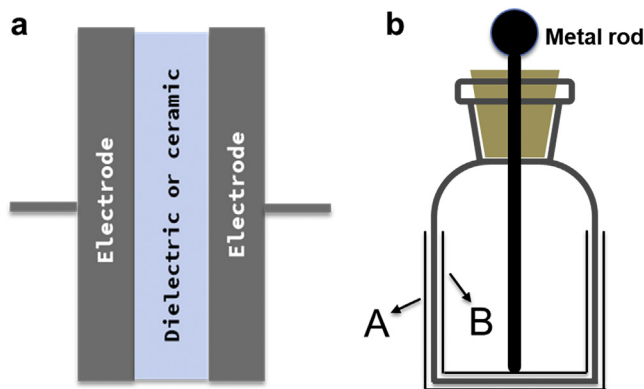
Figure 18.1 (A) Schematic representation of a capacitor design. (B) Cross-sectional representation of Leyden jar (glass jar is loaded with water, metal foils at the inner and outer surfaces are denoted A and B).

where C is a positive proportionality constant called *capacitance*; it signifies the amount of charge needed to induce a specified potential difference between the conducting plates. The physical meaning of capacitance is expressed in terms of charge storage capacity with respect to potential difference (V) between the plates. Dielectric capacitors can exhibit capacitance over a wide range from pico (10^{-12}F) to millifarad (10^{-3} F), as is primarily governed by the nature of the dielectric medium.

Consider a parallel plate capacitor in vacuum, the electric field outside of the planar conductive surface is given by Gauss' law

$$E = \frac{Q}{\varepsilon_0 A} \tag{18.3}$$

Electric potential difference between the plates is given by

$$V = Ed \tag{18.4}$$

$$V = \frac{Qd}{\varepsilon_0 A} \tag{18.5}$$

Since

$$Q = CV \tag{18.6}$$

$$\frac{Q}{C} = \frac{Qd}{\varepsilon_0 A} \tag{18.7}$$

$$C = \frac{Q}{V} = \frac{\varepsilon_0 A}{d} \tag{18.8}$$

Thus, in a medium, capacitance of a capacitor depends on the geometric area (A) of the plates, dielectric constant (ε) of the medium, and distance between the plates (d), given by the following equation

$$C = \frac{\varepsilon \varepsilon_0 A}{d} \tag{18.9}$$

where ε_0 is the permittivity of the vacuum $= 8.8 \times 10^{-12}$ *F/m*, and ε is the relative permittivity of the medium. Thus, charge storage capacity is limited by the dielectric constant, area of the electrodes, and the distance between the electrodes.

3. Historical evolution from capacitors to electrical double-layer capacitors

Historically, a Leyden jar was the first charge storing device, which dates back to 1745 [3]. Due to nature of electrostatic charging, capacitors can store charges rapidly and also discharge very fast. They are considered as power sources which can release pulse power for small periods of time (seconds to milli seconds). Thus, capacitors are suitable power devices in backup circuits of microcomputers and timer circuits for providing periodic charge/discharge cycles. Additionally, the capacitors are being employed in filter units where they can reduce the ripples of dc voltage to meet specific requirements. Though conventional dielectric capacitors are limited by their capacitance values, they are used in frequency filtering applications where the time constant (*τ = RC, R is the resistance and C is the capacitance*) becomes the governing factor.

Electrolytic capacitors are considered as second generation of capacitors. Typically, Al or Ta metals with their insulating oxide layers (through anodization process) serve as a positive or anode terminal. Liquid or gel electrolyte covering on the thin oxide dielectric serves as cathode or negative terminal with metal electrode contacts. Increasing the anode surface area and reducing the thickness of the dielectric layer result in electrolytic capacitors storing more charge ($Q = CV$) per unit volume than dielectric capacitors. Currently, aluminum electrolytic capacitors (AECs) are being employed in filtering out ripples in an electronic circuitry, commonly known as *ac-line filtering*.

Fig. 18.2 outlines the timeline for development of capacitor technologies. H. Becker at General Electrics gets the credit for his pioneering work on electrical double-layer capacitor (EDLC) in 1957. Initial crude EDLC device consisted of porous carbon electrodes dipped in a container of liquid electrolyte; however, this posed a challenge from the commercialization point of view. Further, Robert A. Rightmire at Standard Oil Company of Ohio (SOHIO) optimized EDLC layout by introducing a separator (only allows passage of ions while prevents the electrical shorting of electrodes) between two porous carbon electrodes in sulfuric acid electrolyte. Such kind of optimized format further led interest in researchers in exploring
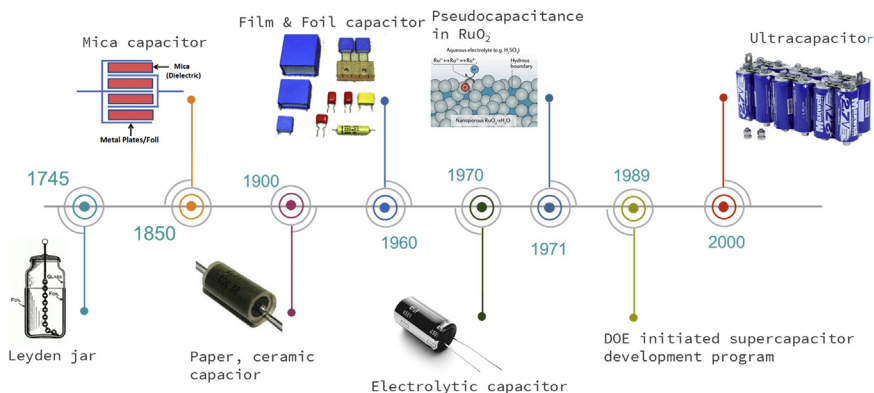
Figure 18.2 Chronological developments from capacitors to supercapacitors. Schematic of pseudocapacitive charge storage of RuO_2 was reproduced from Ref. [4] Copyright 2014 Royal Society of Chemistry.

EDLCs which has resulted in numerous patents and publications. The Japanese company, Nippon Electric Company (NEC), introduced EDLCs into electronics market, as backup power devices for volatile clock chips and complementary metal oxide semiconductor (CMOS) computer memories. During the past few decades, EDLCs expand their usage from portable to transportation sectors, including wireless communication and hybrid electric vehicles (HEVs).

Moving from dielectric capacitors to electrochemical capacitors (Fig. 18.3), there are major differences in electrode materials, design perspective, and operating charge storage mechanisms (Table 18.1). In case of ECs, high-surface-area porous carbon/electrolyte interface replaces the metal/dielectric interface of capacitors. Interfacial capacitance of $10-20$ $\mu F/cm^2$ (based on electrolyte) is recorded for electrical double layers [1]. Thus, typical layout of EDLC includes porous activated carbon electrodes interfacing with electrolyte solution. The electric charge is stored across the
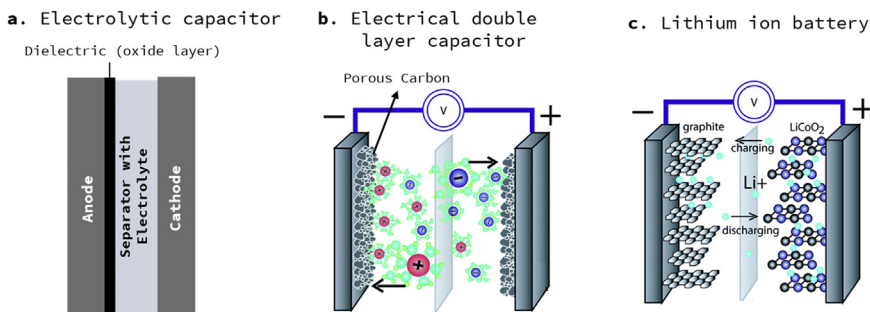
Figure 18.3 Schematic representations for (A) electrolytic capacitor, (B) supercapacitor, and (C) lithium-ion battery.
Reproduced from K. Jost, G. Dion, Y. Gogotsi, Y., Textile energy storage in perspective, J. Mater. Chem. 2 (2014) 10776−10787 Copyright 2014 RSC Publishing.

Table 18.1 Various charge storage features of capacitors, supercapacitors and batteries.

Characteristics	Capacitor	Electrochemical capacitor	Battery
Storage mechanism	Electrostatic	Electrostatic or chemical	Chemical
Charge time	10^{-3}–10^{-6}s	1–10s	>10 min
Life time	>10 years	>10 years	<3 years
E (Wh/kg)	<0.1	5–10	200–270
P (kW/kg)	>10	0.5–20	<10
Charge/Discharge time	10^{-6}-10^{-3} s	Seconds to minutes	minutes to hours
Coulombic efficiency	100%	~100%	<100%
V_{max} limitation	High	Low	Low
Charge storage limited by	Area of electrodes dielectric	Electrode active surface area, nature of electrolyte	Active mass thermodynamics factors
Discharge profile	Linear	Sloping	Plateau
Self-discharge	High	Moderate	Low

E, energy density; P, power density; V_{max}, maximum operation voltage.

electrode/electrolyte interface where the positive and negative charges are separated by the atomic or molecular dimensions of solvent molecules as ultrathin dielectric layers. This interface can store the electric charge through the formation of electrical double layers at electrode/electrolyte interfaces. A pair of electrical double layers is formed on the two electrodes of ECs unlike the single pair of dielectric charge separation in dielectric capacitors. The intrinsic and intricate porous network can act as series of resistor and capacitive elements, with charges stored in a distributed fashion. Theoretically, high surface area carbon materials (1000–3000 m^2/g) should give rise to gravimetric EDL capacitances beyond 300 F/g [C_{dl} ~ 10–20 μF/cm^2 * (1000–3000 m^2/g)] [6–10]. But practically capacitance values are around ~150 F/g and the loss of capacitance could be attributed to inaccessible pores to electrolyte ions and hence partial utilization of surface area for capacitive performance. Inclusion of redox functional groups and heteroatom doping may boost capacitance of carbon materials beyond 200 F/g but energy density remains poor due to limited cell voltage of aqueous electrolytes (1–1.5V). This is due to thermodynamic stability window of aqueous electrolytes. When moving to organic electrolytes, capacitance turns out to be lower in comparison to aqueous electrolytes, but high cell voltage operation (>2 V) contributes to a gain in the energy density as it depends quadratically on V ($E = 1/2CV^2$). Thus, for example, commercial supercapacitors employ organic electrolytes such as tetraethyl ammonium tetrafluoroborate $(C_2H_5)_4N^+$ BF_4^- dissolved in acetonitrile or propylene carbonate, and operate at a cell voltage up to 2.7V [11].

The following table compares different aspects of capacitors, supercapacitors, and batteries.

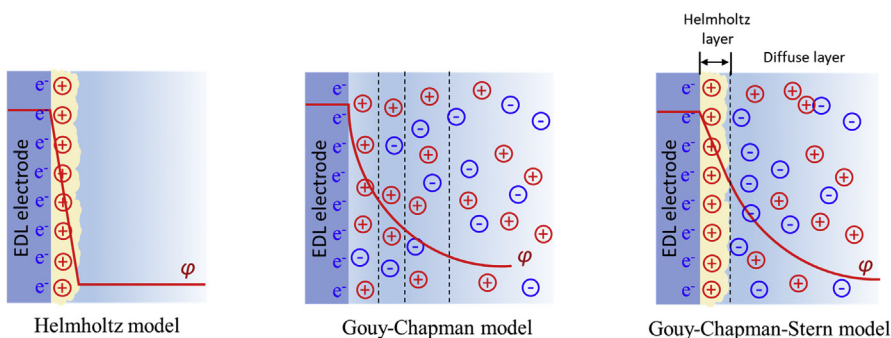# 4. Models to explain electrical double layers

Since there is no charge transfer across electrode/electrolyte interface, the electrical behavior of EDLC is analogous to a capacitor. Oppositely charged ions get accumulated at the electrode/electrolyte interface where the charge on the electrode is confined to <0.1 Å and ions with solvated shells get oriented across such interfaces. The whole array of charged species and oriented dipoles existing across electrode/electrolyte interface is called *electrical double layers*.

Development of the models for interfacial electrical double layer undergoes three classic stages (Fig. 18.4). The double-layer concept originates from the developments of von Helmholtz model on colloidal suspensions [12]. At that time, Helmholtz tried to figure out how the ions and potential distribution near the surface of a solid and liquid (for example, if a metal plate is immersed into the solution). The first theoretical model assumed that any excess charges on a metallic plate remain strictly on the surface, which adsorb counter-ion charges and create charge-separation at interfaces.

The two oppositely charged surfaces, separated by molecular distances, can be considered as a parallel-plate capacitor; as a result, the double-layer capacitance is given by

$$C_{dl} = \frac{\varepsilon \varepsilon_0 A}{d} \tag{18.10}$$

where ε_0 is the vacuum permittivity and ε is the dielectric constant of the medium (here is the electrolyte relative permittivity), A is the surface area of porous carbon electrode, and d is the distance between the ion layer and polarized carbon surface. In Helmholtz model, the capacitance remains a constant for a given chemical system. However, variation of C_{dl} in different electrolyte concentrations was observed experimentally. Thus, Helmholtz model is valid only at specific conditions of concentrated electrolytes, under high potential difference between the electrodes. This model ignores the solvent dynamics and the effects of thermal motion, diffusion, and adsorption of ions into the electrode surface [1].


Figure 18.4 Different models explaining electrical double layers. Red lines show the potential profiles near the surfaces.

To account for thermal motion of ions, Helmholtz model was modified by Gouy and Chapman in early 20th century. In Gouy-Chapman model (Fig. 18.5), the charges on the metallic surface remain strictly on the surface, but this is not the case of the solution. The charges on the metal plate would attract opposite ions and repel carriers with same polarity, which creates a diffuse layer. Diffuse layer consists of counter ions with opposite charge to that of electrode surface. Indeed, there is finite distance needed to counterbalance the charges on the metal plate. To figure out how charges distribute and the length of this diffuse layer (λ_D), let us consider a symmetric binary electrolyte where positive ions and negative ions have same valences Z. We assume that the potential at the surface ($X = 0$) is ζ, which is also called the zeta potential, and the potential at the bulk solution ($X = \infty$) is assumed to be zero, because charges are balanced in the bulk solution.

At any position X, the time-dependent conservation of mass is given by Nernst-Planck equation:

$$\frac{\partial C_\pm}{\partial x} = \nabla \cdot (D_\pm \nabla C_\pm) - \nabla \cdot (\mu_\pm C_\pm E) - \nabla \cdot (u C_\pm) \tag{18.11}$$

where $C_\pm$ is the concentration of positive(+) and negative(−) ions, $D_\pm$ is the diffusion constant, u is velocity of fluid, E is the electrical potential, and $\mu_\pm$ is the "mobility" or the potential of the particle's drift velocity to an applied force. At equilibrium, no mass
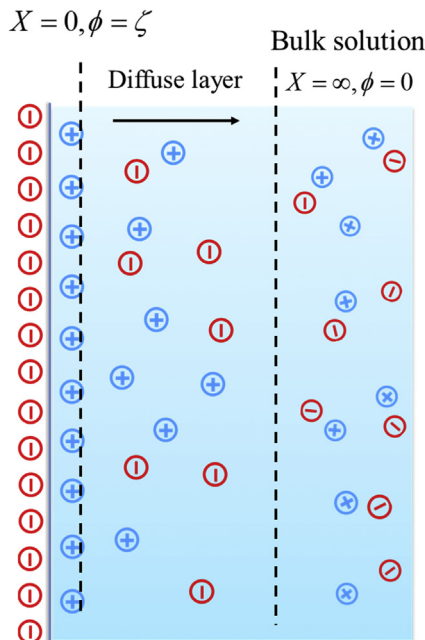
Figure 18.5 View of the ion distribution near the surface of electrode and aqueous solution in Gouy-Chapman model.

exchange takes place at any positions, and there is no convection because there is no solvent flow. So Eq. (18.11) can be rewritten as:

$$\nabla \cdot (D_\pm \nabla C_\pm) - \nabla \cdot (\mu_\pm C_\pm E) = 0 \tag{18.12}$$

To simplify the problem, we consider the case of the two-dimensional situation; in such case, E is given by:

$$E_x = -\frac{d\phi}{dx} \tag{18.13}$$

Eq. (18.12) is then:

$$\frac{d}{dx}\left(\mu_\pm C_\pm \frac{d\phi}{dx} + D_\pm \frac{d}{dx}C_\pm\right) = 0 \tag{18.14}$$

Boundary conditions for solving Eq. (18.14) is given by $\frac{d\phi}{dx} = 0$, $\frac{dC_\pm}{dx} = 0$ at $x = \infty$. Then

$$\mu_\pm C_\pm \frac{d\phi}{dx} + D_\pm \frac{d}{dx}C_\pm = 0 \tag{18.15}$$

Consider Nernst-Einstein Relation:

$$D = \frac{\mu kT}{Ze} \tag{18.16}$$

Eq. (18.15) is then:

$$\frac{Z_\pm e}{kT}C_\pm \frac{d\phi}{dx} + \frac{dC_\pm}{dx} = 0 \tag{18.17}$$

Then

$$C_\pm = C_0 \exp\left[-\frac{Z_\pm e}{kT}\phi\right] \tag{18.18}$$

where C_0 is the concentration of bulk solution. On the other side, the distribution of potential is given by Poisson-Boltzmann equation:

$$\frac{d^2\phi}{dx^2} = \frac{-\rho_f}{\varepsilon} = \frac{-ZF(C_+ - C_-)}{\varepsilon} \tag{18.19}$$

Noting that C_+ and C_- are given by Eqs. (18.18), (18.19) can be rearranged as:

$$\frac{d^2\phi}{dx^2} = \frac{C_0 Z F}{\varepsilon}\left[\exp\left(\frac{Ze\phi}{kT}\right) - \exp\left(-\frac{Ze\phi}{kT}\right)\right] = \frac{2ZFC_0}{\varepsilon}\sinh\left(\frac{Ze\phi}{kT}\right) \qquad (18.20)$$

For ideal solutions, at Debye-Huckle approximation when $\frac{Ze\phi}{kT} \ll 1$. The Taylor series further simplifies Eq. (18.20) :

$$\frac{d^2\phi}{dx^2} = \frac{C_0 Z F}{\varepsilon}\left[\left(1 + \frac{Ze\phi}{kT}\right) - \left(1 - \frac{Ze\phi}{kT}\right)\right] = \frac{2ZFC_0}{\varepsilon}\frac{Ze\phi}{kT} = \frac{2(Ze)^2 N_A C_0}{\varepsilon kT}$$

$$(18.21)$$

where $\phi(x=0) = \zeta$ and $\phi(x=\infty) = 0$.

Debye length λ_D, also known as the length of diffusion layer, is defined as:

$$\lambda_D = \sqrt{\frac{\varepsilon kT}{2(Ze)^2 N_A C_0}} \qquad (18.22)$$

Eq. (18.21) can then be rearranged as:

$$\frac{d^2\phi}{dx^2} = \frac{\phi}{\lambda_D^2} \qquad (18.23)$$

Finally, potential can be solved as:

$$\phi = \zeta e^{-x/\lambda_D} \qquad (18.24)$$

The electric potential reduces in magnitude by $1/e$ at every Debye length. The thickness of the diffusion layers varies with the concentrations of the electrolytes. For a solution with water medium ($\varepsilon \approx 80\varepsilon_0$) the length of the diffusion layer can be calculated as:

$$\lambda_D = \sqrt{\frac{1}{Z^2 \times C_0}} \times 9.7\text{nm} \qquad (18.25)$$

and ions distribution can be solved from Eqs. (18.18) and (18.24):

$$C_\pm \approx C_0\left(1 \mp \frac{Ze\phi}{kT}\right) = C_0\left(1 \mp \frac{Ze\zeta}{kT}e^{-x/\lambda_D}\right)$$

$$\left(\text{For positive ions, } C_+ = C_0\left(1 - \frac{Ze\zeta}{kT}e^{-x/\lambda_D}\right)\right)$$
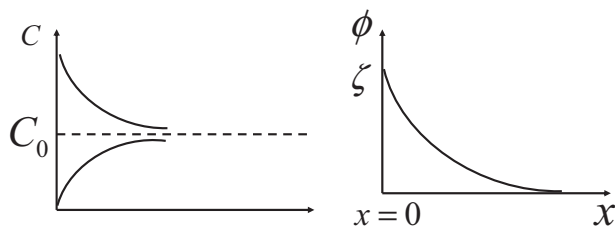
$$(18.26)$$

Figure 18.6 Ions distribution and potential profiles through the diffuse layer in the Gouy-Chapman model.

Eq. (18.26) describes the ion distribution in the diffuse layer in a general way, positive and negative ions decay away from/to the surface exponentially. At large potential ϕ (highly charged surface), the drop is abrupt, the diffuse layer becomes compact; while at smaller potential, the decay is more gradual (Fig. 18.6).

The Gouy-Chapman model is the most classic model to describe the electrical double layer, and it has been continually used in various fields until now [13,14]. However, this model does not account for ion-ion correlations. The main success of this model lies in the accurate estimations of ionic profiles near planar and curved surfaces at low concentrations of electrolytes. When dealing with multivalent charged ions and high charge density surfaces, Gouy-Chapman model fails to explain the interfacial processes.

By combining the approaches of Helmholtz model with the more refined Gouy-Chapman model, Stern model proposed organization of ion distribution across the electrode/electrolyte interface into two regions—a compact layer of charges at the inner region (Stern layer) and a diffuse layer at the outer region. Therefore, resultant double-layer capacitance can be given by

$$1/C_{dl} = 1/C_H + 1/C_{diff}$$

In a concentrated electrolyte, the Debye length approaches to zero, turning C_{diff} to infinity, so that double-layer capacitance $C_{dl} \sim C_H$. The Helmholtz model is good enough for ECs with high concentrated electrolytes.

In case of symmetric full cell supercapacitors, two electrical double layers are assumed to be connected in series through a resistor (Fig. 18.7). The equivalent circuit is given by an RC circuit.

Therefore, capacitance (C) of an EDLC is given by

$$(C)^{-1} = (C_+)^{-1} + (C_-)^{-1}$$

where C_+ corresponds to capacitance of positive and C_- corresponds to capacitance of negative electrodes.
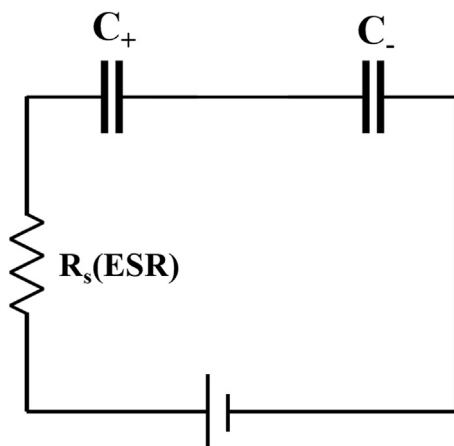
Figure 18.7 Circuit model for EDLCs, two interfaces constitute the two capacitors in series and electrolyte behaves as a resistor.

5. Evolution of electrode materials for supercapacitors

Supercapacitors are broadly classified into (i) electrical double-layer capacitors that involve physical charge storage mechanism without charge transfer and (ii) pseudo(faradaic) capacitors that involve rapid redox reactions with charge transfer across electrode-electrolyte interface.

Porous materials are the key for developing electrical double-layer capacitors. Typically, cavities, channels, interstices, or defects are sites for accommodation of electrolyte ions. Based on IUPAC nomenclature, pores are broadly classified into (i) micropores (pore widths <2 nm), (ii) mesopores (2−10 nm), and macropores (>10 nm) [15]. High surface area porous carbon electrodes interfacing the electrolytes have shown to benefit from the (i) increase of surface area and (ii) decrease of distance between the charged layers, leading to overall boost of capacitance by orders of magnitude compared to conventional capacitor technologies employing metal plates. However, activated carbon electrodes may not be optimal electrode material as they have distribution of pore sizes and volumes. Chmiola et al. have demonstrated that by controlling the pore sizes matching that of electrolyte ions, solvation shell strips off facilitating bare ion entry to the nanopores (<1 nm) [16]. Such kind of controlled pore size of carbon materials were synthesized by precise etching of metal atoms from their corresponding metal carbide precursors. Conventional models explaining EDL behavior at micropores have become less effective in the case of carbide-derived carbons. It was found that normalized capacitance decreases until a critical value of pore size of 1 nm followed by an unusual rise of capacitance values. Due to restrictions in the formation of Helmholtz and diffuse layers at sub nanometric pores, ion desolvation leading to the collapse of solvation shell promoting bare ion interaction with the carbon surface explains the anomalous increase in the capacitance [16]. Largeot et al. demonstrated that matching of pore size to the

size of bare ion results in maximum capacitance due to stripping off of solvation shell [17]. Unexpectedly, anomalous increase in the capacitance at nanometer or subnanometer pores is solely attributed to the desolvation effects. However, the cost of processing such carbide-derived carbons has limited their commercialization, and activated carbons derived from coconut shells are being employed in commercial supercapacitors. Nonetheless, an in-depth understanding on the matching of pore size to the size of electrolyte ions gave a clue for carbon manufacturers to control the pore size of activated carbon in the nanometric range. Thus, commercial EDLCs achieved an energy density up to 10 Wh/kg, which is a twofold increment in comparison to EDLC devices back in 2005.

Carbon is a versatile element due to its tunable morphologies and properties. Moreover, its high abundance and low specific weight make carbon attractive for energy storage applications (Table 18.2). For instance, carbon nanotubes and carbon black are often employed as conductive additives for processing of electrodes as they distribute charge over the entire thickness of the electrode while helping the efficient charge transport 3D pathways. One-dimensional nanomaterials including carbon nanotubes and carbon nanofibers have been employed as electrodes for double-layer capacitors [19−22]. Again, double-layer capacitance (C_{dl}) is often limited to the specific surface area of the electrodes and hence $C_{dl} = C_A \times SSA$ where C_A is the specific area capacitance and SSA is the specific surface area. Sometimes, internal micropores (<2 nm) are difficult to be accessed by the electrolyte ions and accessible electrochemical active surface area may be further limited.

Although supercapacitor electrodes can be assembled in different styles (Fig. 18.8A and B), the basic unit consists of two metal collectors (each coated with the active electrode materials), an ion-permeable insulating separator, and the aqueous or organic electrolytes. The basic structure can be stacked to form a flat pouch cell or rolled into a radial structure, and the size depends on the capacitance and voltage requirements. A detailed analysis of the cost of different components of the cell including the cost ranges for electrode materials, separators, electrolyte, and production cost revealed that the cost variations stem from each component (Fig. 18.8C). The cost of the current collector dominates in the manufacturing of supercapacitors, as well as the expensive organic solvent (in this case, N-methyl-2-pyrrolidone) used for

Table 18.2 Most commonly used carbon materials for supercapacitor applications [18].

| Electrode material	SSA (m²/g)	C (F/g)		
		Aqueous	Organic	Ionic liquids
Activated carbons	1000−3000	200−400	100−150	100−150
Templated carbons	500−2500	120−350	120−135	150
Carbon nanotubes	120−500	20−180	20−80	20−45
Carbon-derived carbons	1000−1600	−	100−140	100−150
Carbon blacks	250−2000	<300	−	−
Aerogels/Xerogels	400−1000	40−220	<160	−
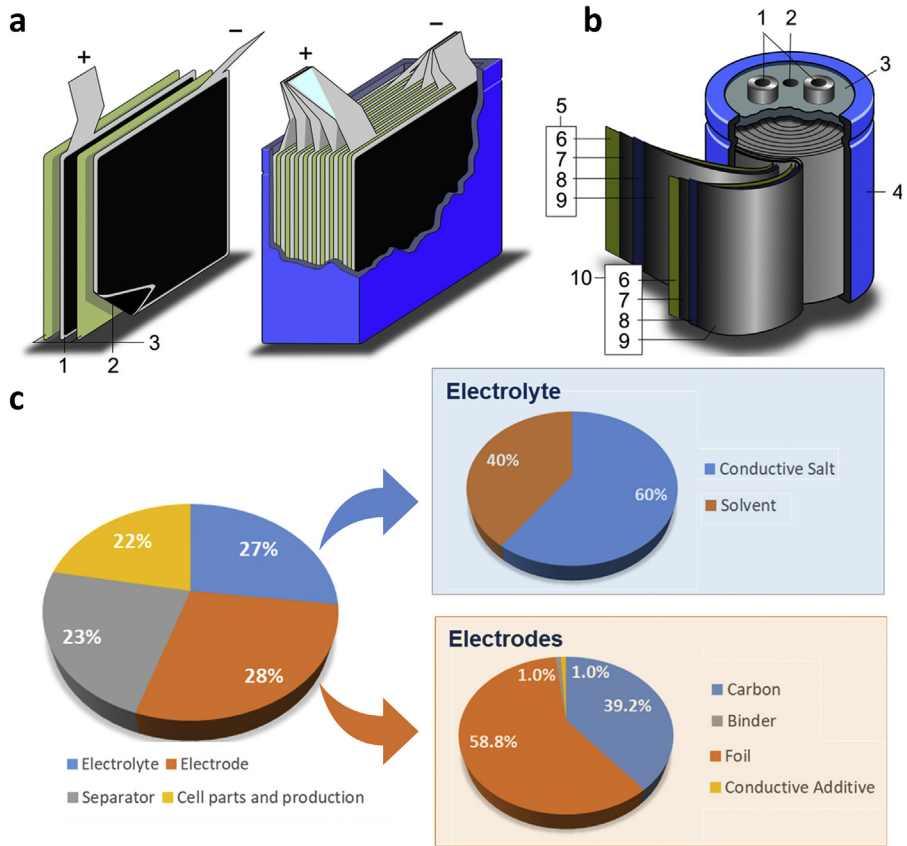
Figure 18.8 Different formats of supercapacitors. (A) Stacked supercapacitors; the structure includes (1) positive electrode and (2). negative electrode, (3) porous separator.
(B) Radial-style supercapacitor, the construction of such device requires packaging of different parts including (1) terminals, (2) safety vent, (3) sealing disc, (4) aluminum can, (5) positive pole, (6) separator, (7). carbon electrode, (8) collector, (9) carbon electrode, (10) negative pole.
(C) Production cost analysis for different parts of a supercapacitor cell, including electrode, electrolyte, and passive components.

forming the paste of active electrode materials. In the case of electrolyte, the conductive salt contributes a major part (60%) to the total cost. It should also be noted that those estimations refer to a cylinder carbon-based supercapacitor; the estimates will depend on the architectural style and the electrode material.

6. State-of-the-art energy storage technologies

A Ragone plot displays the snapshot of state-of-the-art energy and power performance metrics of different energy technologies (Fig. 18.9). Based on thermodynamics and
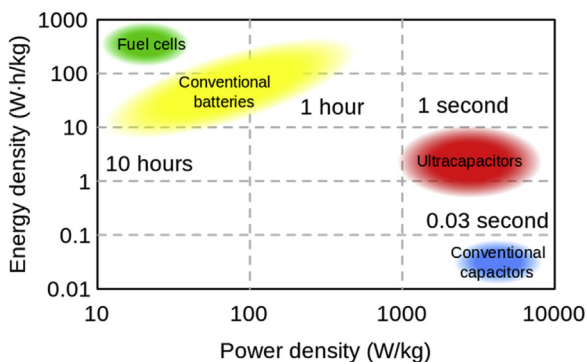
Figure 18.9 The Ragone plot showing the energy and power performance metrics of a variety of electrochemical energy storage devices.

kinetics of charge storage processes, a tradeoff between energy and power densities is inherent in any given energy storage technology. It is worth mentioning that the energy and power performance of energy storage devices has been normalized by the total weight (gravimetric) or volume of entire cell. However, laboratory testing cells often report material-level performance and should not be compared with that of commercial scale devices. The only comparison that can be made is charging/discharging time (ratio of energy density to power density) between laboratory test cells versus commercial devices. Furthermore, operational time scales are often used where supercapacitors deliver stored energies in a few seconds; this is much faster than for batteries. At charging time scales of a few seconds, supercapacitors can store more energy compared to batteries. In principle, batteries may be operated in a high-power mode but cycling life could significantly reduced due to loss of energy and coulombic efficiencies. In this scenario, pseudocapacitive materials have shown promise as they offer fast charge-discharge rates over batteries and higher capacities over double-layer capacitors. Again, surface confined redox reactions, ultrafast ion intercalation induced redox reactions at fast charging rates contribute to the simultaneous achievement of energy and power. Apart from development of new electrode materials with new mechanisms of charge storage, there have been efforts to design new configurations of energy storage devices [9,23,24]. For instance, asymmetric supercapacitors employ pairing double-layer electrodes with redox electrodes to achieve higher voltage operation and hence superior energy and power performance over symmetric supercapacitors. Similarly, it is possible to develop hybrid energy storage devices by pairing up electrolytic electrodes with double-layer electrodes to improve power performance.

7. Pseudocapacitive energy storage

7.1 Understanding of pseudocapacitance

Pseudocapacitive charge storage exploits the surface redox and fast intercalation redox processes for high rate energy storage. The prefix "pseudo" signifies to "it appears to be"

in the context that kinetic behavior resembles that of a typical EDLC. Pseudocapacitance in which capacitance is due to Faradaic reactions is distinctly different from double-layer capacitance (due to physical electrostatic charge storage), as well as structural and phase transformations associated with the battery electrodes. Electrical double layers formed at the electrode/electrolyte interface are often limited by the active surface area for storing charges. The EDLs formation and relaxation (µs-ns) happens at much faster time scales compared to redox reactions (10^{-2}-10^{-4} s).

Though electrochemical kinetics resembles the kinetics in a capacitor, the mechanism of charge storage is based on fast redox (Faradaic) reactions [4]. Sometimes the boundaries between EDLCs, pseudocapacitors, and batteries may look blurred; it is often important to correctly classify the category and hence report appropriate electrochemical performance metrics for the constructive progress of the field [25,26]. Typically, the experimental estimation of capacitance for pseudocapacitive materials cannot be simply explained by $C_{dl} = C_A \times SSA$. This first observation provides a clue to finding out the charge storage mechanism to explain the observed capacitance value. Box-like cyclic voltammograms (RuO_2, MnO_2) and broad redox peaks with mirror-like appearance (T-Nb_2O_5 and $Ti_3C_2T_x$ MXene) are typically observed in current versus potential response plots of pseudocapacitive materials. Further, current response versus scan rate analysis provides an estimate for charge storage kinetics. Ideally, pseudocapacitive materials possess short diffusion pathways for the ions with charging time scales similar to that of capacitors without involving any phase transformations by continuous operation over number of cycles. Electrochemical impedance spectroscopy measurements offer distinct features based on kinetics of charge storage phenomenon. Pseudocapacitive materials typically show vertical imaginary impedance at low frequency, signifying the absence of solid-state diffusion [27,28].

Historically in 1960s, pseudocapacitance was introduced to explain the underpotential deposition and hydrogen adsorption reactions. In the energy storage perspective, pseudocapacitance was employed in distinguishing the charge storage kinetics of hydrous RuO_2 thin films versus single crystals of RuO_2. [29] It was found that although electrochemical kinetics resembled that of a capacitor, but mechanism of charge storage was based on continuous change of Ru oxidation state. The important point to be noted is that pseudocapacitors exhibit electrochemical kinetics which is same as capacitors while the mechanism of charge storage is somewhat like battery-based materials. Thus, pseudocapacitive materials bridge the gap between supercapacitors and batteries in the Ragone chart. With the advent of nanostructured materials, the boundaries among three categories have been blurred; however, caution must be practiced in identifying and reporting the electrochemical performance metrics accurately for the constructive progress of the EES field. Despite the Faradaic nature of charge storage phenomenon, fast and reversible surface redox reactions are responsible for capacitive type response, which in turn satisfies linearity of the extent of charge (ΔQ) to associated potential change (ΔE). The redox active centers must obey the condition of surface confinement (located near the surface of the metal oxides, at a distance, $\ll (2Dt)^{1/2}$, where D is the diffusion coefficient for charge-compensating ions (cm^2/s) and t is the diffusion time range (s) to eliminate

the limitations associated with bulk diffusion-limited processes). Thus, pseudocapacitive materials exhibit electrochemical performance intermediate between EDLCs and batteries [30].

7.2 Classification of pseudocapacitance

Pseudocapacitance is broadly classified into (i) intrinsic, if it is independent of the particle sizes and thickness of the electrode materials (underpotential deposition or surface/intercalation redox reactions) and (ii) extrinsic, which arises due to nano-structuring of typical battery electrodes, as shown in Fig. 18.10.

(i) Underpotential deposition—accumulated ions at electrode-electrolyte interface which can be deposited at positive potentials to their redox potentials. Examples include protons on Pt and Pd^{2+} ions on Au surface.

$$M + xC^{z+} + xze^- \leftrightarrow C_xM \quad (M = Pt \text{ or } Au; \; C \text{ is adsorbed atom H or Pd})$$
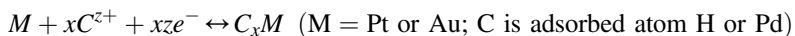
where number of absorbed atoms = x.valence of the absorbed atoms = z number of transferred electrons = zx.

A very high specific capacitance value beyond 1 mF/cm^2 can be achieved, but low potential window of operation (~ 0.5 V) limits their energy density.

(ii) Redox pseudocapacitance—near-surface confined redox reactions

Examples: RuO_2, MnO_2, and conducting polymers.

$$Ox \; + \; zC^+ + ze^- \leftrightarrow RedC_z$$
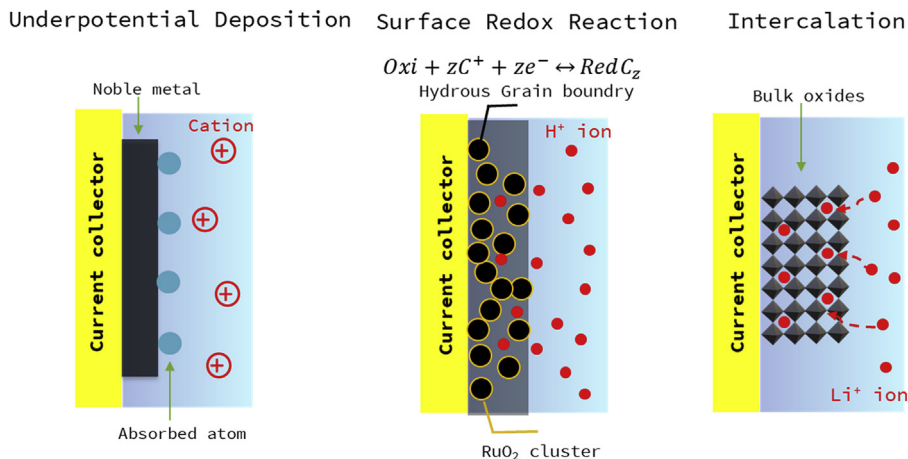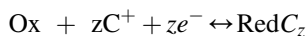
Figure 18.10 Capacitive features may be expected for different types of Faradaic mechanisms.

where C is the surface-absorbed electrolyte cation C^+ (H^+, K^+, Na^+) and z is the number of transferred electrons. The maximum volumetric capacitance is estimated to be around 5 kF/cm^3, which is much larger than ~ 0.8 F/cm^3 (double-layer capacitance of 1 cm^3 of a compact high surface area carbon).

(iii) Intercalation pseudocapacitance—ions intercalate into redox materials through fast diffusing channels without having solid-state diffusion limitations. Examples include Nb_2O_5 and $Ti_3C_2T_x$ MXene. This mechanism is considered similar to battery electrodes; however, fast electrochemical response kinetics with long cycling stability makes them distinctly different from battery electrodes.

$$MA_y +\ xLi^+ + xe^- \leftrightarrow Li_xMA_y$$
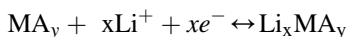
8. Material requirements for achieving simultaneous high energy density at high power density

Given the limited energy density of porous carbon electrodes, new types of materials may need to have the following characteristics [31]:

(i) High density of accessible redox active sites, (ii) high electronic conductivity, (iii) short diffusion pathways for ions transport, (iv) reversible redox reactions. Especially, nanomaterials with increased surface area-to-volume ratio may provide high density of redox active sites with short ion diffusion pathways.

RuO_2 and MnO_2 are well-known pseudocapacitive materials, where the redox change of transition metal in valence are balanced by the electrosorption/desorption of cations from the electrolyte. Since only surface redox reactions are involved in this case, charge storage kinetics resemble that of a capacitor with superior cycling stability and no phase transformations unlike batteries that exploit bulk Faradaic reactions.

It is recommended to report capacity values (coulombs or mAh normalized by weight, area, or volume) for pseudocapacitive materials. However, when the voltammograms are rectangular and charge-discharge profiles are linear (as in the case of RuO_2 and MnO_2), capacitance can be calculated using linear equations. For example, Nb_2O_5 and $Ti_3C_2T_x$ MXene exhibit broad redox peaks on capacitive envelop; the average value of capacitance can be estimated by integration formula rather than linear equations. Nanostructured nickel oxides, hydroxides, and cobalt oxides and hydroxides that exhibit sharp redox peaks, which are well separated, should not be classified under pseudocapacitive materials. So, caution must be exercised in classification and reporting of charge storage performance of electrode materials.

Most of the pseudocapacitive materials do exhibit redox charge storage behavior in aqueous electrolytes, thus limiting the voltage window of operation. Dunn group investigated T-Nb_2O_5 in Li-ion containing nonaqueous electrolytes [32]. Linear dependence of current on scan rate, absence of phase transformations, broad redox peaks with little separation on top of capacitive envelop make Nb_2O_5 distinctly different from battery-like electrodes. Due to fast diffusive 2D pathways, this material

is classified under "intercalation induced pseudocapacitive," which exhibited a capacity of 150 mAh/g at high rates. Similarly, $Ti_3C_2T_x$ MXene electrodes showed Li-ion capacity up to 130 mAh/g in LiTFSI/PC electrolyte. By careful control of surface chemistry of MXenes electrodes [33], charge storage capacities up to 200 mAh/g were achieved. Both, Nb_2O_5 and $Ti_3C_2T_x$ could be potential replacement for low-capacity carbon materials in the design of hybrid metal-ion capacitor devices.
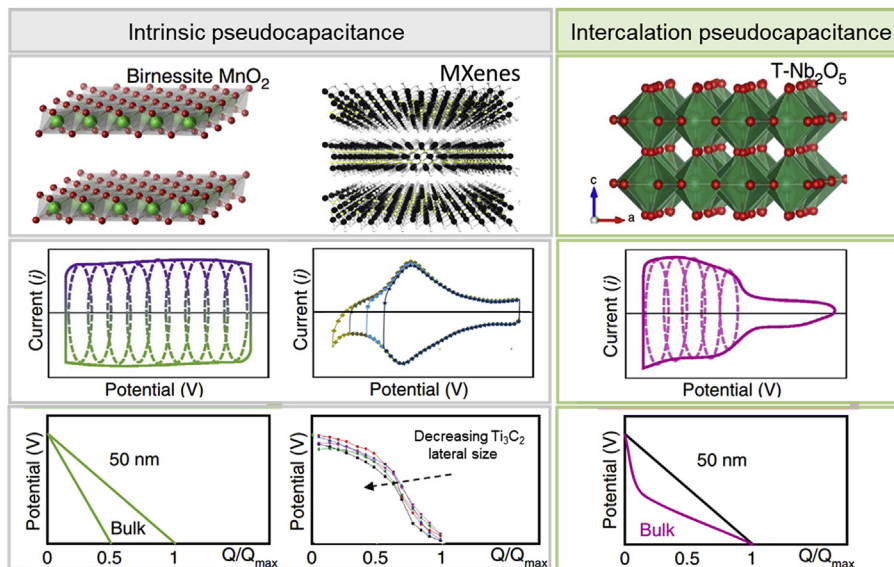
Thus, pseudocapacitive materials bridge the performance gap between EDLCs and batteries. The common goal for both communities lies in the development of high-rate and high-energy devices. There have been some efforts in transforming battery materials into pseudocapacitive type by reducing the particle size or nanostructuring. For example, $LiCoO_2$ and $LiFePO_4$ battery electrodes, exhibit constant plateaus in their galvanostatic charge-discharge profiles. By reducing the size of $LiCoO_2$ and introducing defects in $LiFePO_4$ materials, sloping type profiles (typical for pseudocapacitive electrodes) were observed [34]. Thus, it is a nice strategy in improving energy density of ECs while exceeding power density of batteries. However, long-term cycling tests need to be run to evaluate their sustainable performance.

Given the geometric advantages of 2D materials, MoS_2, WS_2, 2D oxides, carbides, nitrides, MOFs have been extensively investigated as electrodes for supercapacitors (Fig. 18.11). Restacked 2D materials offer gallery sites for accommodation of ions without undergoing significant volumetric changes. Past decade has witnessed the exploration of 2D materials that exhibit a rare combination of metallic conductivity and redox charge storage properties. The largest family of 2D materials comprised of transition metal carbides, nitrides, carbonitrides—MXenes—have shown high rate pseudocapacitive charge storage properties [35]. Specifically, titanium carbide MXene ($T_3C_2T_x$) showed proton-induced pseudocapacitive behavior in protic electrolytes and often shows stable electrochemical performance in the negative potential windows. This further led to the replacement of low capacitive negative carbon electrodes in the design of high energy density asymmetric supercapacitors. In a classic study, positive RuO_2 electrode was paired with negative MXene electrode. As both the electrodes have redox activity in acidic electrolyte with complementary potential windows of operation and hence the operating cell voltage turned out to be beyond the thermodynamic electrochemical splitting of water; more details can be found in Section 10.4.

9. Electrochemical characterization techniques for supercapacitors

9.1 Cyclic voltammetry

Cyclic voltammetry (CV) is a kind of transient potentiodynamic technique that can study the electrochemical behavior for an electrochemical cell or in three-electrode setups. CV techniques are widely used in the field of supercapacitors to determine (1) voltage window of the electrode material in given electrolyte, (2) reversible or nonreversible couples (3) Diffusion coefficient of the ions across solid electrode materials where Nernstian equilibrium is maintained.

Figure 18.11 Summary of the characteristic metrics for typical types of 2D pseudocapacitive materials.
Reproduced from M.R. Lukatskaya, B. Dunn, Y. Gogotsi, Multidimensional materials and device architectures for future hybrid energy storage. Nat. Commun. 7 (2016) 1−13 Copyright 2016 Springer Nature.

From CV curves, information about equivalent series resistance and leakage resistance can also be roughly quantified by comparing different shapes. Taking an ideal capacitor, for example, Fig. 18.12A, since capacitance is strictly constant, perfect rectangular CV shape is retained. When an equivalent series resistance (ESR) is introduced in series with the ideal capacitor (Fig. 18.12B), a deviated CV curve appears. ESR can
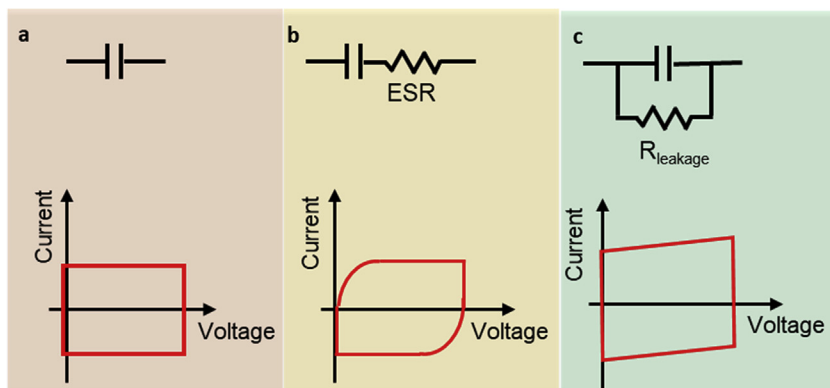
Figure 18.12 Current-voltage profiles for different RC circuit models.

be introduced due to many factors including intrinsic resistances of electrode and electrolytes, interfacial contact resistance between electrode and current collector, or resistance from separator. The slow increase of the current results from the stabilization of the current at the beginning. Leakage resistance is another type of resistance that can be commonly observed; it usually causes the self-discharge phenomenon for a device. In such cases, a slope of the current versus voltage can be observed when the CV scan is performed (Fig. 18.12C). Ideally, the leakage resistance should be as large as possible.

CV scans can also be performed to estimate the capacitance. Mathematically, the capacitance C (Farad, F) is given by the ratio of charge in the system to the corresponding change of applied potential:

$$C(V) = \frac{i(V)dt}{dV} \tag{18.27}$$

Capacitance $C(V)$ is dependent on the voltage. For cyclic voltammetry measurements, dV/dt is nothing but scan rate ν and capacitance is expressed in the voltage domain as

$$C(V) = \frac{i(V)}{\nu} \tag{18.28}$$

Then the integrated charge values with respect to the potential range provides an estimate for the average capacitance

$$\overline{C} = \frac{\int_{V_1}^{V_2} C(V)dV}{\int_{V_1}^{V_2} dV} = \frac{\int_{V_1}^{V_2} \frac{i(V)}{\nu} dV}{V_2 - V_1} = \frac{\int_{V_1}^{V_2} i(V)dV}{\nu * (V_2 - V_1)} \tag{18.29}$$

9.2 Galvanostatic charge-discharge

Galvanostatic charge-discharge technique allows one to measure change of potential with respect to time up on charging at a constant current value. For an ideal capacitor, a linear current response can be observed (Fig. 18.13A) and the CD curves are
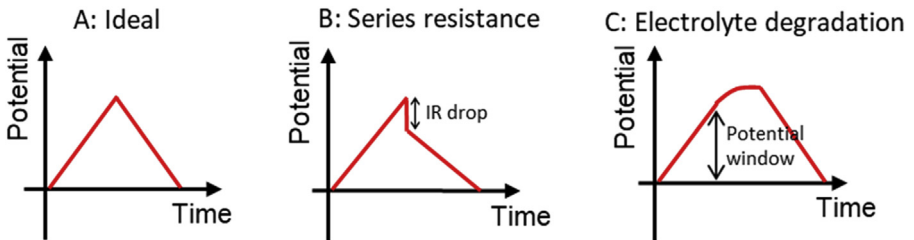
Figure 18.13 Galvanostatic charge-discharge profiles of supercapacitors with ideal behavior (A), iR drop due to series resistance (B), and overcharging leading to the degradation of electrolyte (C).

perfectly symmetric with charging time (t_c) is equal to discharging time (t_d) and ratio (t_d/t_c) is called coulombic efficiency, which should be $\sim 100\%$ for supercapacitors. The capacitance can simply be calculated by deriving the slope $\left(\frac{\Delta V}{\Delta t}\right)$ of the charge/discharge curve:

$$C = \frac{I\Delta t}{\Delta V} \tag{18.30}$$

When the electrode has internal resistance, an abrupt drop of the potential will be observed due to the IR drop (Fig. 18.13B). And this internal resistance is often correlated to the resistance measured from EIS data. Charge-discharge curves also tell the stability of the electrolyte; when electrolyte degradation happens, obvious plateaus can be observed, and gas evolution can also be observed experimentally at this stage (Fig. 18.13C).

9.3 Electrochemical impedance spectroscopy

Electrochemical impedance spectroscopy (EIS) measures the properties of the system in a quasi-equilibrium state; it measures the response of voltage or current by applying a small ac sinusoidal signal [36]. Because it can sweep the frequencies, separate physical properties of the systems such as mass transport, charge transfer, and chemical reactions can be estimated at different reaction steps.

A classic model for a supercapacitor is shown in Fig. 18.14A, where interfacial resistance is connected in parallel with the capacitor, and this RC circuit is connected in series with the electrolyte resistance R_s (also called equivalent series resistance (ESR)).

At high frequency limit ($\omega \to \infty$), the impedance of the model is calculated to be:

$$Z = \left[Z_{Re} - \left(R_s + \frac{R_{ct}}{2}\right)\right]^2 + R_{im}^2 = \left(\frac{R_{ct}}{2}\right)^2 \tag{18.31}$$
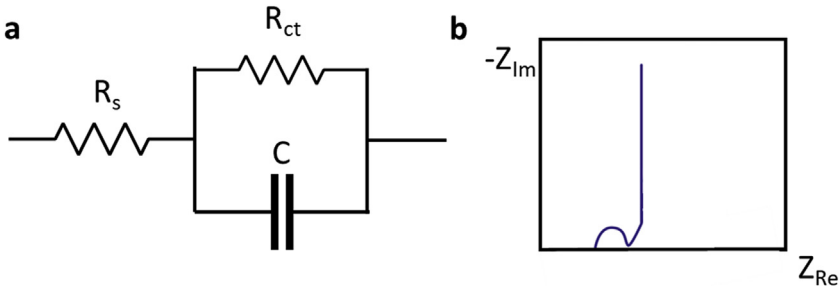
Figure 18.14 Equivalent Randles circuit of as EDLC (A) and its corresponding Nyquist plot (B).

Thus, the elliptic equation in the Nyquist plot results in a semicircle shape (Fig. 18.14B), where intercept in the X-axis is the internal resistance and diameter of the semicircle is the interfacial charge transfer resistance. For typical supercapacitors, semicircle in the high frequency region of spectrum is absent. In some cases, presence of semicircle for EDLCs causes confusion among the community. This is probably due to interfacial impedance across the current collector/electrode interface rather than the charge transfer resistance across the electrode/electrolyte interface. By recording impedance spectra at different dc potentials along with a small ac sinusoidal potential perturbation (5−10 mV), charge transfer resistance can be distinguished from interfacial impedance [36]. It is worth noting that the semicircle may be absent for an ideal supercapacitor, where there is no interfacial charge transfer reactions. Porous electrode behavior is characterized by the slope line which is inclined at 45 degree angle to X-axis. At low frequency regime, near vertical behavior of imaginary part of impedance signifies the capacitive response.

9.4 Energy density and power density calculations

Strictly speaking, energy and power densities must be calculated for devices but not for individual electrodes. Three-electrode measurements help in evaluating specific capacitance, potential, rate performance, and cycling stability of the materials with the promise of using them in constructing energy storage devices. For a full cell, Energy (Joule, J) stored in the device can be assessed by measuring the current $i(t)$ and voltage $V(t)$ in a given time (from t_1 to t_2) as:

$$E = \int_{t_1}^{t_2} i(t)V(t)dt \tag{18.32}$$

Normally, the unit of energy is converted to Wh/kg by dividing it by a factor of 3.6. Eq. (18.32) can be separately solved both from cyclic voltammetry and galvanostatic charge-discharge measurements. In the case of cyclic voltammetry, a fixed rate of voltage change over time gives:

$$V(t) = V_0 + vt \tag{18.33}$$

where V_0 is the initial voltage in the positive scan and v is the scan rate (V/s). Then Eq. (18.32) can be solved as:

$$E = \frac{\int_{V_1}^{V_2} i(V)VdV}{v} \tag{18.34}$$

where V_2 and V_1 are the corresponding voltages at given times. In a full CV scan, energy from charge and discharge process can be separately calculated by integrating

the corresponding areas. In contrast, in a galvanostatic charge-discharge test, the current is fixed, then Eq. (18.32) can be easily solved as:

$$E = i \int_{t_1}^{t_2} V(t)dt \qquad (18.35)$$

Eq. (18.35) can be easily calculated by the integration of the charge/discharge curves.

In both cases, an averaged power (Watt, W) of the device can be estimated by:

$$P = \frac{E}{t_2 - t_1} \qquad (18.36)$$

Often, positive and negative electrodes (2-electrode configuration) are assembled in either sandwich or interdigitated fashion to demonstrate the energy and power performance metrics of the 2-electrode cell. Most of the laboratory cells often normalize performance with respect to weight (or volume) of active electrode materials, but not including the passive components weight or volume. So, care must be taken when comparing the performance of laboratory test devices with that of packaged cells, which incorporates total stack weight or volume for estimating performance metrics. Corresponding energy/power densities are also easily obtained by dividing total energy/power by mass or volume. Linear formula $\left(E = \frac{1}{2}CV^2 \right)$ for estimating energy and power performance is only applicable to capacitive-type profiles (rectangle CV shape or linear GCD curve). When CVs and GCDs distort from ideal behavior, integration formula must be employed rather overestimating them by using linear equations [37]. Rate performance, cycling stability, coulombic and energy efficiencies are estimated from galvanostatic charge-discharge data.

10. Energy storage devices

10.1 On-chip energy storage

Miniaturized electronics and emerging Internet of things (IoT) could demand for microscale energy storage devices toward advancement of wireless sensor networks and self-powered systems (Fig. 18.15A). Compatible integration of these energy storage devices ensures the sustainable operations of the maintenance-free functional electronic devices such as implantable biochips, radio frequency identification (RFID) tags, and integrated smart devices.

Commercial thin film batteries and microbatteries satisfy energy density requirements, but low power density and limited life time remain the major bottlenecks for long-term operation. Microsupercapacitors—new generation of supercapacitors—are considered to be replacement for microbatteries as they can have infinite life time with higher power densities, which could open the way to maintenance-free integrated
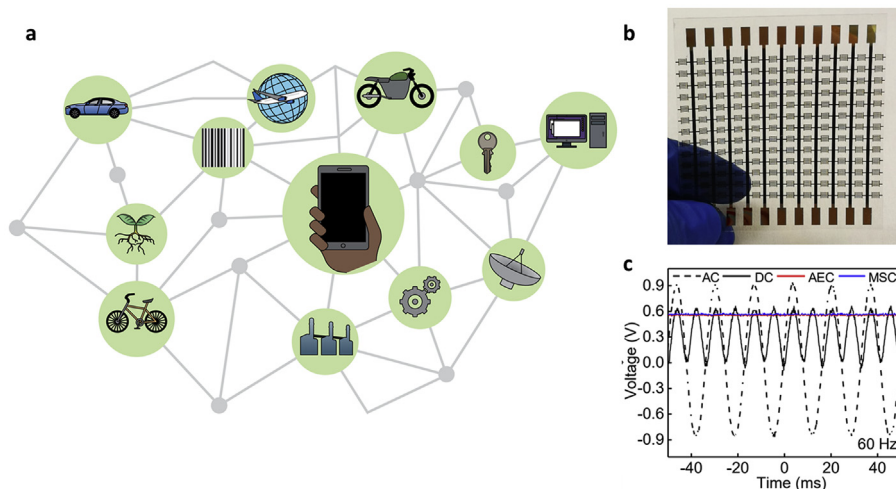
Figure 18.15 (A) Schematic of network web of sensors used for emerging IoT. Reprinted with permission from Ref. [38]. Copyright 2019 Springer Nature. (B) Large-scale micro-supercapacitors on flexible substrate and (c) Output voltage signal after filtering using the microsupercapacitor.
Reprinted with permission from Q. Jiang, N. Kurra, K. Maleski, Y. Lei, H. Liang, Y. Zhang, H.N. Alshareef, On-chip MXene microsupercapacitors for AC-line filtering applications. Adv. Energy Mater. 9 (2019) 1901061. Copyright 2019 Wiley.

devices. In addition, microsupercapacitors are more suited for self-powered sensor and device applications. In such devices, the power source (such as triboelectric nanogenerators) provides voltage buses intermittently. A constant voltage source is required for charging up batteries, but a supercapacitor can be charged employing nonconstant voltage supplies. Typical layout of microsupercapacitor may include either thin film or planar interdigitated electrode architecture where the latter may have advantage including free movement of electrolyte ions offering high power and rate capabilities over their sandwich counterparts.

This field of microsupercapacitors is evolving rapidly. There have been excellent review articles describing the progress of microsupercapacitors [23,40−44]. A number of research articles focusing on developing fabrication strategies and deposition of electrode materials in coplanar electrode design. Numerous carbonaceous materials including activated carbon, carbide-derived carbon, onion-like carbon, carbon nanotubes, graphene, and aerogels have been employed as electrode materials in microsupercapacitors. Due to the nature of electrostatic charge storage in carbon materials, pseudocapacitive materials have been employed for improving capacitance values. A variety of transition metal oxides (RuO_2, MnO_2), conducting polymers, and transition metal carbides and nitrides were explored for microsupercapacitors. Similar to the development of electrode materials from carbonaceous materials to pseudocapacitive type for improving capacitance values, microsupercapacitors employing pseudocapacitive materials showed higher energy density values over those employing carbonaceous materials.

10.2   Micropower sources for filtering applications

One of the key aspects of microsupercapacitors is to replace bulky aluminum electrolytic capacitors in ac-line filtering applications. The important design aspect lies on the choice of open structured electrodes with interdigitated design to enable high frequency operation of microsupercapacitors. While high surface area electrodes such as activated carbons may suffer from the internal porosity, which makes them with operational time response of typically 1s. However, for filtering applications, specifically 120 Hz ac waveform can be filtered only if the capacitor has an RC time constant of 8.3 ms. Technically, phase angle versus frequency response should be maintained at a phase angle of -90 degrees until 120 Hz frequency. Nonporous carbon materials including vertically grown graphene, carbon nanotubes, and carbon blacks have shown their high frequency operation (until 120 Hz) with capacitive response. Pioneering work by John Miller laid foundations for developing EDLCs for ac-line filtering applications.

Some of the pseudocapacitive materials including conducting polymers and titanium carbide MXenes showed frequency response matching that of Al-electrolytic capacitors (Fig. 18.15B and C). This is due to high electronic conductivity and ionic conductivity of electrode materials besides the coplanar layout of electrodes. Research directions may continue to employ microsupercapacitors as compatible ac-line filters and micropower units for on-chip electronics.

10.3   Integrated microsupercapacitors

Furthermore, to meet the mobility requirements of different multitudes of sensors in the emerging internet of things (IoTs), a lot of effort is focused on integrating on-chip energy storage devices as micropower sources for bio/gas sensors, etc. Some of the energy harvesting units including triboelectric generator were integrated with microsupercapacitors for formulating self-powered microsystems (Fig. 18.16A and B). Microsupercapacitors have also been integrated with thin film transistors for simpler circuits control compared with traditional transistor transducers (Fig. 18.16C). Thanks to its merits such as light weight, small size, and customizable structure choice, integrated microsupercapacitors can be deployed in various application scenes (Fig. 18.16D). Energy and power density in a given footprint area are two key performance merits for a microsupercapacitor; conventional microfabrication techniques with carbon-based materials show limited areal energy density [22,47−49]. To improve the areal energy and power performance metrics of microsupercapacitors, 3D microsupercapacitors were fabricated to have increased areal loading in a given foot-print area [50]. For large-scale production, those microsupercapacitors can be fabricated through development of functional inks with optimal rheological properties and prototyping them by various printing technologies such as screen printing, inkjet printing, 3D printing, roll-to-roll techniques, *etc*.
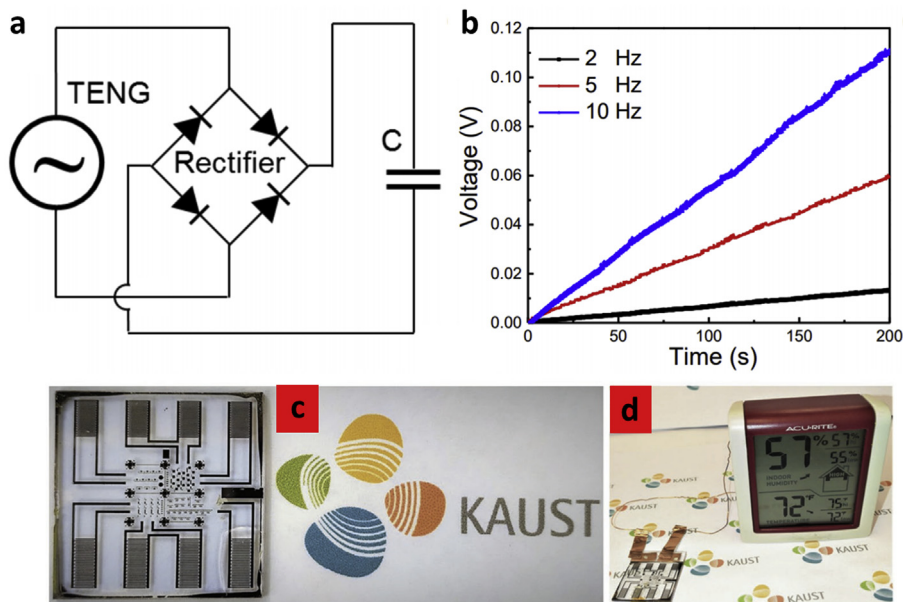
Figure 18.16 Integrated microsupercapacitors for self-powered sensors and electronics. (A) Circuit diagram of the self-powered system. (B) Charging profiles of the microsupercapacitor employing triboelectric nanogenerator (TENG) at various frequencies. Optical image of the integrated microsupercapacitor and transistor device, with the (C) KAUST logo. (D) Powering off a commercial hygro-thermometer device by the chip.
(B) Reprinted with permission from Q. Jiang, C. Wu, Z. Wang, A.C. Wang, J.H. He, Z.L. Wang, H.N. Alshareef, MXene electrochemical microsupercapacitor integrated with triboelectric nanogenerator as a wearable self-charging power unit. Nanomater. Energy, 45 (2018) 266−272. Copyright 2018 Elsevier. (D) Reprinted with permission from Ref. M.K. Hota, Q. Jiang, Z. Wang, Z.L. Wang, K.N. Salama, H.N. Alshareef, Integration of electrochemical microsupercapacitors with thin film electronics for on-chip energy storage. Adv. Mater. 31 (2019) 1807450. Copyright 2019 Wiley.

10.4 Hybrid supercapacitors

The amount of charge that can be stored and delivered from an energy storage device is primarily dependent on the nature of charge storage mechanism of electrode materials, architecture, and device configuration. Inherent tradeoff always exists between energy and power performance of different energy storage technologies; and are often worked out through design of new materials, hybrid configurations, and device layouts.

By exploiting the complementary potential windows of operation of two different electrode materials in a common electrolyte, asymmetric supercapacitors can be operated at voltage windows beyond the thermodynamic decomposition potentials of electrolytes (Fig. 18.17). By pairing two pseudocapacitive materials with balanced charge
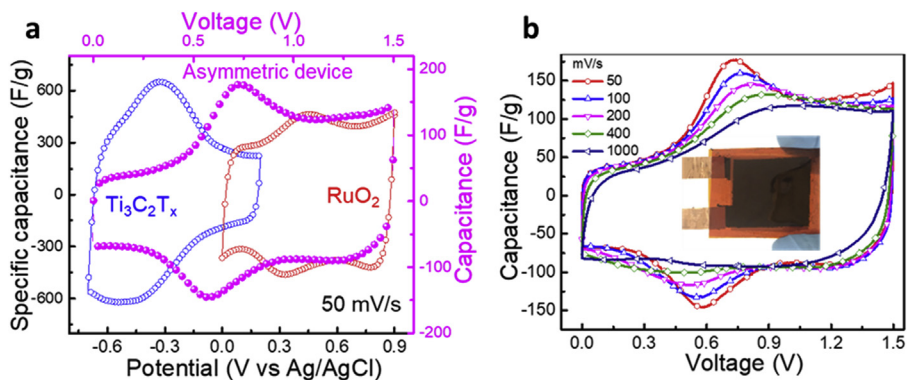
Figure 18.17 All pseudocapacitive $RuO_2//Ti_3C_2T_x$ asymmetric device: (A) Cyclic voltammograms of RuO_2, $Ti_3C_2T_x$electrodes, and the asymmetric device at a scan rate of 50 mV/s (B) CVs of $RuO_2//Ti_3C_2T_x$ asymmetric sandwich device at various scan rates from 50 to 1000 mV/s, inset shows the digital photograph of the asymmetric device.
Reprinted with permission from Q. Jiang, N. Kurra, M. Alhabeb, Y. Gogotsi, H.N. Alshareef, All pseudocapacitive MXene-RuO_2 asymmetric supercapacitors. Adv. Energy Mater. 8 (2018) 1703043. Copyright 2019 Wiley.

storage capacity and rate performance, one can eliminate the limited capacity and rates offered by negative carbon electrodes. One of the best examples reported is the constructing of asymmetric supercapacitors using an MXene negative electrode with a RuO_2 positive electrode. The resulting device can operate at a voltage of 1.5 V and at high rates (1 V/s). Energy limitations associated with the symmetric supercapacitors can be overcome by design of asymmetric supercapacitors, as energy is proportional to square of voltage window of the device.

10.5 Hybrid metal-ion capacitors

Hybrid electrochemical capacitors combine Faradaic (battery or pseudocapacitive) electrodes with capacitive electrodes. The concept of hybrid capacitor takes advantage of the high energy density of battery-type electrode and the high-power density of capacitive electrodes. The name of the hybrid capacitors depends on the shuttling (or rocking) of associated metal-ions (lithium, sodium, potassium, *etc.*) between the positive and negative electrodes. Typical examples include Li-ion capacitor combining intercalation anode (a prelithiated graphite) with adsorption type cathode (porous carbon). Prelithiation of graphite ensures not only the formation of stable SEI layer but also hosting sufficient Li-ions for long-term operation of lithium ion capacitor (LIC). The operating cell voltage of 3.8−2.2 V of LIC with long lifespan and short charge/discharge time (several minutes) [52] are the attractive features over batteries.

The operating cell voltage is determined by the potential range of both electrodes. Negative (positive) electrodes should have the lowest (highest) average potential, thus leading to high cell voltage and energy density of the hybrid device (Fig. 18.18).
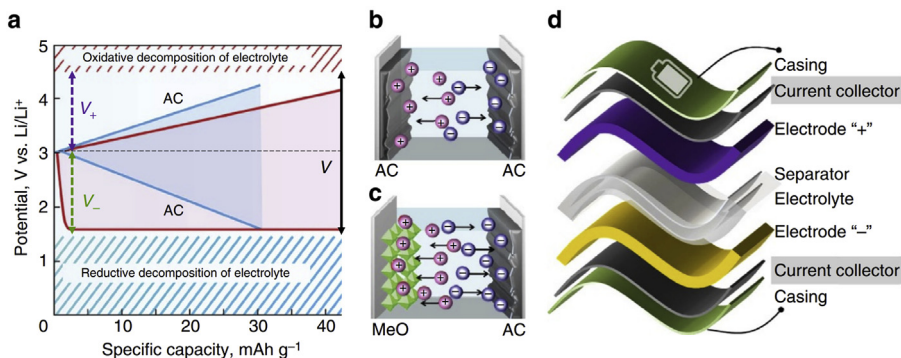
Figure 18.18 Hybrid capacitor versus symmetric supercapacitor. (a) Electrode potentials (V_+ and V_-) and cell voltages of devices (V) versus specific capacity for symmetric (blue lines) and hybrid (red lines) devices. Electrode configurations for (b) symmetric supercapacitor and (c) hybrid capacitor are presented separately. (d) Components of a commercial full cell. Reprinted with permission from M.R. Lukatskaya, B. Dunn, Y. Gogotsi, Multidimensional materials and device architectures for future hybrid energy storage. Nat. Commun., 7 (2016) 1−13. Copyright 2018 American Chemical Society.

However, low potential operation of negative electrodes may suffer from the Li or metal plating issues during fast charging rates. Formation of stable SEI layer is another challenging task in such cases. So, it is very important to develop matching electrode/electrolyte combinations to minimize the parasitic reactions and improve the first cycle coulombic efficiency. In the case of cathode, it is always challenging to match the specific capacitance of activated carbon to the high capacity anodes. Taking lessons from the investigations on supercapacitors, optimization strategies must be done towards controlling the electrical conductivity of active materials, the specific surface areas, pore size distributions, surface modifications, and novel capacitive energy storage mechanisms such as pseudocapacitance.

11. Applications of supercapacitors

By the nature of charge storage mechanism, supercapacitors are power devices which can supply rapid power in a limited time scale. Supercapacitors can complement energy devices including batteries and fuel cells where there is a requirement of pulse power supply for long periods of time while saving life times of energy devices (Fig. 18.19). In China and Japan, supercapacitors are used in emergency doors of air buses. The idea is to create zero emission mobility through the usage of supercapacitors. At each station halt, 15−20 s charging time may be sufficient for a drive of 2 km until the next charging station stop. Due to the high power capabilities of supercapacitors, energy can be captured from regenerative braking systems, which can be reused during the startup of a car or bus. The combination of diesel and electrical energy storage from supercapacitors has been demonstrated to save energy in a
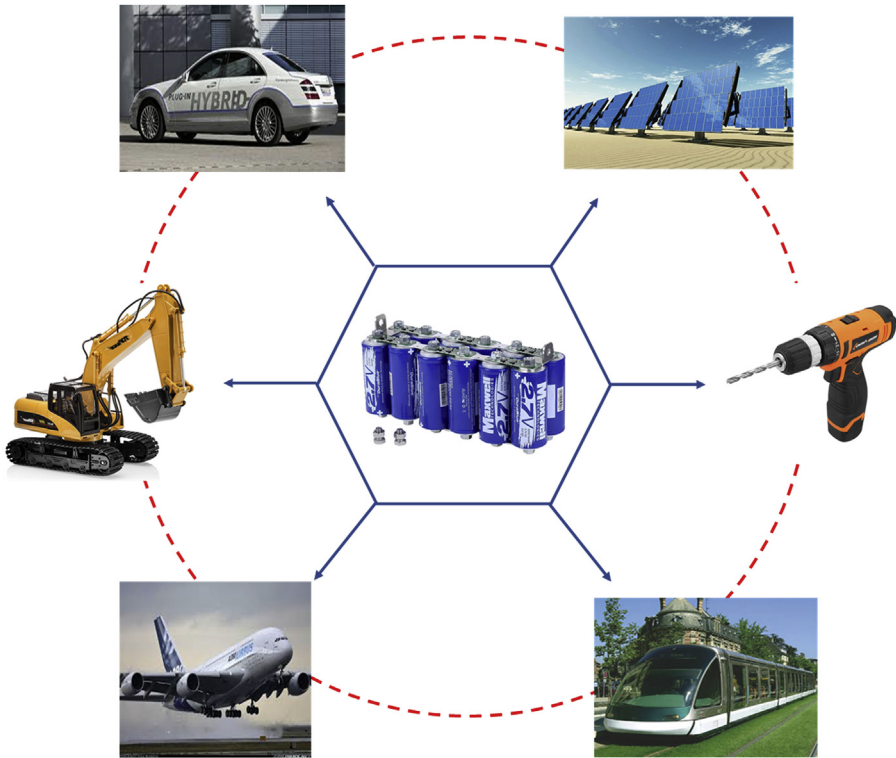
Figure 18.19 Various practical applications for supercapacitors.

number of successful programs [18]. Moreover, continuous improvements have been made to further increase the energy densities of supercapacitors. Recently, Shenzhen Toomen New Energy reported their new graphene-based supercapacitors in a trade show, the product was claimed to have a milestone energy density of $60-80$ Wh/kg and can be charge/discharged $10-20$ times faster than commercial lithium-ion batteries. The improved energy density was attributed to the combination of metal oxide electrode and graphene electrode. Moreover, the cell can operate in a wide temperature range of $-40°C$ to $80°C$.

Worldwide sales of supercapacitors are about USD 400 million in the past decade, and this number is projected to increase to USD 720 million by 2025 [53]. The compound annual growth rate (CAGR) from 2020 to 2025 is expected to be more than 12.0%, the growth of supercapacitor market is driven by the rising applications in electrical cars, trains, and airplanes. As of 2019, Tesla (USA), Nippon Chemi-Con (Japan), CAP-XX (Australia), LS Mtron (South Korea), and Panasonic (Japan) were the major players in the supercapacitor market. In contrast, from 2020 to 2027, the market for batteries will grow from USD 108.4 billion at a CAGR of 14.1% [54], among which the largest segment is lithium-ion products. Such large market growth is attributed to the high demand from the automotive applications.

Although the market for supercapacitors is still a small niche market that is not keeping pace with battery market, the encouraging factor comes from reduction in prices of supercapacitors, which cost around US$0.01 per farad or US$2.85 per kilojoule and is expected to drop down further in the mid term. The low price and increasing demand for large-scale energy harvesting applications may further fuel the supercapacitor market in the near future. Recently, supercapacitors are also being deployed for grid-scale energy storage applications. For example, Maxwell Technologies provides grid-scale supercapacitor solutions for distributed energy storage utilities and industrial sites; moreover, solar rooftops equipped with supercapacitors are also being designed to meet the home energy requirements and to cut greenhouse gas emissions [55].

12.   Conclusions and challenges

Supercapacitors are energy efficient devices with high power capability and can last long periods (millions of charge/discharge cycles) without failure. Batteries often have limitations associated with sluggish diffusion of ions through bulk materials and hence eventually lead to resistive losses in the form of heat or sometimes dendrites formation when aimed for high power applications. This is a major safety concern that has been witnessed by Tesla electric car and the Dremaliner airplane (made by Boeing) [56,57]. Thus, supercapacitors are suitable for a range of applications including renewable energy and grid storage integrations, capturing energy through regenerative braking of electric vehicles, and light trail. Further developments of EDLCs may be possible through understanding the nature of electrode/electrolyte interfaces in the viewpoint of ion fluxes, ion dynamics, and ion arrangement at micropores. Employing redox-active electrolytes may further contribute to the improved capacitive performance of EDLCs. Ion fluxes and ions adsorption at nanometric pores have been thoroughly investigated by numerous in-situ characterization methods employing spectroscopy tools (infrared, nuclear magnetic resonance (NMR)), scattering techniques (Raman, neutron, and X-ray), mass spectrometry, and modelling studies. Ion dynamics and adsorption during operation were studied using electrochemical quartz-crystal microbalance (EQCM) and electrochemical atomic force microscopy (EC-AFM) [58].

Development of high voltage (>4 V) electrolytes and modifying electrode/electrolyte interfaces through formation of ionically conductive passive layers could improve the energy performance of EDLCs. Exploitation of fast redox charge storage characteristics of transition metal compounds and conducting polymers is clearly a road map for achieving high energy and high power simultaneously.

Self-discharge and heat managements are the main concerns of supercapacitor technology. A charged supercapacitor discharges on its own due to charge recombination events associated with either diffusion of ions from the site of double layers to bulk electrolyte or leakage through functional groups or traces of impurities of water in the organic electrolytes. Heat is generated through high power mode operation, which needs to be properly managed for long-term operation of supercapacitors.

Screening of new electrode compositions and structures with development of new electrolyte formulations could benefit in advancing fast charging electrochemical energy storage devices. New conductive salt/solvent and electrode/electrolyte combinations may be screened employing machine learning and artificial intelligence which provide roadmap for experimentalists for the practical design of optimal configurations toward improvement of electrochemical performance. More in-depth studies should focus on understanding the ion arrangement and charge transfer events at electrode/electrolyte interfaces.

References

[1] B.E. Conway, Electrochemical Supercapacitors: Scientific Fundamentals and Technological Applications, Springer Science & Business Media, 2013.

[2] J.Z. Buchwald, R. Fox (Eds.), The Oxford Handbook of the History of Physics, OUP, Oxford, 2013.

[3] J.L. Heilbron, Electricity in the 17th and 18th Centuries: A Study of Early Modern Physics, Univ of California Press, 1979.

[4] V. Augustyn, P. Simon, B. Dunn, Pseudocapacitive oxide materials for high-rate electrochemical energy storage, Energy Environ. Sci. 7 (2014) 1597−1614.

[5] K. Jost, G. Dion, Y. Gogotsi, Textile energy storage in perspective, J. Mater. Chem. 2 (2014) 10776−10787.

[6] O. Kuzmina, J.M. Slattery, M. Hu, Q. Song, S. Jiao, G.M. Haarberg, X. Yue, Improvements of energy conversion and storage: general discussion, Faraday Discuss 190 (2016) 291−306.

[7] A. Lewandowski, P. Jakobczyk, M. Galinski, Capacitance of electrochemical double layer capacitors, Electrochim. Acta 86 (2012) 225−231.

[8] Y. Wang, Y. Song, Y. Xia, Electrochemical capacitors: mechanism, materials, systems, characterization and applications, Chem. Soc. Rev. 45 (2016) 5925−5950.

[9] A. Vlad, N. Singh, C. Galande, P.M. Ajayan, Design considerations for unconventional electrochemical energy storage architectures, Adv. Energy Mater. 5 (2015) 1402115.

[10] G. Wang, L. Zhang, J. Zhang, A review of electrode materials for electrochemical supercapacitors, Chem. Soc. Rev. 41 (2012) 797−828.

[11] C. Zhong, Y. Deng, W. Hu, J. Qiao, L. Zhang, J. Zhang, A review of electrolyte materials and compositions for electrochemical supercapacitors, Chem. Soc. Rev. 44 (2015) 7484−7539.

[12] J.B. Allen, R.F. Larry, Electrochemical Methods Fundamentals and Applications, John Wiley & Sons, 2001.

[13] M. Liu, Y. Pang, B. Zhang, P. De Luna, O. Voznyy, J. Xu, E.H. Sargent, Enhanced electrocatalytic CO_2 reduction via field-induced reagent concentration, Nature 537 (2016) 382−386.

[14] D. Liu, X. Li, S. Chen, H. Yan, C. Wang, C. Wu, L. Song, Atomically dispersed platinum supported on curved carbon supports for efficient electrocatalytic hydrogen evolution, Nat. Energy 4 (2019) 512−518.

[15] J. Rouquerol, D. Avnir, C.W. Fairbridge, D.H. Everett, J.M. Haynes, N. Pernicone, K.K. Unger, Recommendations for the characterization of porous solids (Technical Report), Pure Appl. Chem. 66 (1994) 1739.

[16] J. Chmiola, G. Yushin, Y. Gogotsi, C. Portet, P. Simon, P.L. Taberna, Anomalous increase in carbon capacitance at pore sizes less than 1 nanometer, Science 313 (2006) 1760−1763.

[17] C. Largeot, C. Portet, J. Chmiola, P.L. Taberna, Y. Gogotsi, P. Simon, Relation between the ion size and pore size for an electric double-layer capacitor, J. Am. Chem. Soc. 130 (2008) 2730−2731.

[18] E. Frackowiak, F. Béguin, Supercapacitors: Materials, Systems and Applications, Wiley-VCH Verlag GmbH & Co, Poznan, 2013.

[19] M. Beidaghi, C. Wang, Micro-supercapacitors based on interdigital electrodes of reduced graphene oxide and carbon nanotube composites with ultrahigh power handling performance, Adv. Funct. Mater. 22 (2012) 4501−4510.

[20] P. Huang, C. Lethien, S. Pinaud, K. Brousse, R. Laloo, V. Turq, P. Simon, On-chip and freestanding elastic carbon films for micro-supercapacitors, Science 351 (2016) 691−695.

[21] D. Pech, M. Brunet, P.L. Taberna, P. Simon, N. Fabre, F. Mesnilgrente, H. Durou, Elaboration of a microstructured inkjet-printed carbon electrochemical capacitor, J. Power Sources 195 (2010) 1266−1269.

[22] D. Pech, M. Brunet, H. Durou, P. Huang, V. Mochalin, Y. Gogotsi, P. Simon, Ultrahigh-power micrometre-sized supercapacitors based on onion-like carbon, Nat. Nanotechnol. 5 (2010) 651−654.

[23] D. Qi, Y. Liu, Z. Liu, L. Zhang, X. Chen, Design of architectures and materials in in-plane micro-supercapacitors: current status and future challenges, Adv. Mater. 29 (2017) 1602802.

[24] M.R. Lukatskaya, B. Dunn, Y. Gogotsi, Multidimensional materials and device architectures for future hybrid energy storage, Nat. Commun. 7 (2016) 1−13.

[25] Y. Jiang, J. Liu, Definitions of pseudocapacitive materials: a brief review, Energy Environ. Mater. 2 (2019) 30−37.

[26] S. Fleischmann, J.B. Mitchell, R. Wang, C. Zhan, D.E. Jiang, V. Presser, V. Augustyn, Pseudocapacitance: from fundamental understanding to high power energy storage materials, Chem. Rev. 120 (2020) 6738−6782.

[27] Y. Gogotsi, R.M. Penner, Energy storage in nanomaterials−capacitive, pseudocapacitive, or battery-like? ACS Nano 12 (2018) 2081−2083.

[28] B.E. Conway, Transition from "supercapacitor" to "battery" behavior in electrochemical energy storage, J. Electrochem. Soc. 138 (1991) 1539.

[29] S. Ardizzone, G. Fregonara, S. Trasatti, "Inner" and "outer" active surface of RuO_2 electrodes, Electrochim. Acta 35 (1990) 263−267.

[30] C. Choi, D.S. Ashby, D.M. Butts, R.H. DeBlock, Q. Wei, J. Lau, B. Dunn, Achieving high energy density and high power density with pseudocapacitive materials, Nat. Rev. Mater. 5 (2020) 5−19.

[31] P. Simon, Y. Gogotsi, Materials for electrochemical capacitors, Nat. Mater. 7 (2010) 845−854.

[32] V. Augustyn, J. Come, M.A. Lowe, J.W. Kim, P.L. Taberna, S.H. Tolbert, B. Dunn, High-rate electrochemical energy storage through Li+ intercalation pseudocapacitance, Nat. Mater. 12 (2013) 518−522.

[33] J.L. Hart, K. Hantanasirisakul, A.C. Lang, B. Anasori, D. Pinto, Y. Pivak, M.L. Taheri, Control of MXenes' electronic properties through termination and intercalation, Nat. Commun. 10 (2019) 1−10.

[34] M. Okubo, E. Hosono, J. Kim, M. Enomoto, N. Kojima, T. Kudo, I. Honma, Nanosize effect on high-rate Li-ion intercalation in LiCoO2 electrode, J. Am. Chem. Soc. 129 (2007) 7444−7452.

[35] M. Okubo, A. Sugahara, S. Kajiyama, A. Yamada, MXene as a charge storage host, Acc. Chem. Res. 51 (2018) 591−599.

[36] P.L. Taberna, P. Simon, J.F. Fauvarque, Electrochemical characteristics and impedance spectroscopy studies of carbon-carbon supercapacitors, J. Electrochem. Soc. 150 (2003) 292.

[37] T.S. Mathis, N. Kurra, X. Wang, D. Pinto, P. Simon, Y. Gogotsi, Energy storage data reporting in perspective—guidelines for interpreting the performance of electrochemical energy storage systems, Adv. Energy Mat. 9 (2019) 1902007.

[38] P. Simon, Y. Gogotsi, Perspectives for electrochemical capacitors and related devices, Nat. Mater. 19 (2020) 1151−1163.

[39] Q. Jiang, N. Kurra, K. Maleski, Y. Lei, H. Liang, Y. Zhang, H.N. Alshareef, On-chip MXene microsupercapacitors for AC-line filtering applications, Adv. Energy Mater. 9 (2019) 1901061.

[40] G. Xiong, C. Meng, R.G. Reifenberger, P.P. Irazoqui, T.S. Fisher, A review of graphene-based electrochemical microsupercapacitors, Electroanalysis 26 (2014) 30−51.

[41] M. Beidaghi, Y. Gogotsi, Capacitive energy storage in micro-scale devices: recent advances in design and fabrication of micro-supercapacitors, Energy Environ. Sci. 7 (2014) 867−884.

[42] A. Tyagi, K.M. Tripathi, R.K. Gupta, Recent progress in micro-scale energy storage devices and future aspects, J. Mater. Chem. 3 (2015) 22507−22541.

[43] Z.S. Wu, X. Feng, H.M. Cheng, Recent advances in graphene-based planar micro-supercapacitors for on-chip energy storage, Nat. Sci. Rev. 1 (2014) 277−292.

[44] N.A. Kyeremateng, T. Brousse, D. Pech, Microsupercapacitors as miniaturized energy-storage components for on-chip electronics, Nat. Nanotechnol. 12 (2017) 7−15.

[45] Q. Jiang, C. Wu, Z. Wang, A.C. Wang, J.H. He, Z.L. Wang, H.N. Alshareef, MXene electrochemical microsupercapacitor integrated with triboelectric nanogenerator as a wearable self-charging power unit, Nanomater. Energy 45 (2018) 266−272.

[46] M.K. Hota, Q. Jiang, Z. Wang, Z.L. Wang, K.N. Salama, H.N. Alshareef, Integration of electrochemical microsupercapacitors with thin film electronics for on-chip energy storage, Adv. Mater. 31 (2019) 1807450.

[47] P. Huang, D. Pech, R. Lin, J.K. McDonough, M. Brunet, P.L. Taberna, P. Simon, On-chip micro-supercapacitors for operation in a wide temperature range, Electrochem. Commun. 36 (2013) 53−56.

[48] D. Qi, Z. Liu, Y. Liu, W.R. Leow, B. Zhu, H.,. Yang, X. Chen, Suspended wavy graphene microribbons for highly stretchable microsupercapacitors, Adv. Mater. 27 (2015) 5559−5566.

[49] B. Hsia, M.S. Kim, M. Vincent, C. Carraro, R. Maboudian, Photoresist-derived porous carbon for on-chip micro-supercapacitors, Carbon 57 (2013) 395−400.

[50] Q. Jiang, N. Kurra, C. Xia, H.N. Alshareef, Hybrid microsupercapacitors with vertically scaled 3D current collectors fabricated using a simple cut-and-transfer strategy, Adv. Energy Mater. 7 (2017) 1601257.

[51] Q. Jiang, N. Kurra, M. Alhabeb, Y. Gogotsi, H.N. Alshareef, All pseudocapacitive MXene-RuO2 asymmetric supercapacitors, Adv. Energy Mater. 8 (2018) 1703043.

[52] M.S. Park, Y.G. Lim, J.H. Kim, Y.J. Kim, J. Cho, J.S. Kim, A novel lithium-doping approach for an advanced lithium ion capacitor, Adv. Energy Mater. 1 (2011) 1002−1006.

[53] Supercapacitor Market by End Use Industry, https://www.lucintel.com/supercapacitor-market.aspx (accessed January 25, 2021).

[54] Battery Market Size & Share, https://www.grandviewresearch.com/industry-analysis/battery-market (accessed January 25, 2021).

[55] The Microgrid Way: Going Green with Solar & Supercapacitor-based Energy Storage, https://microgridknowledge.com/supercapacitor-based-energy-storage/(accessed February 15, 2021).

[56] Dreamliner Battery Type Requires Safeguards, Safety Advocate Says, 2013. https://edition.cnn.com/2013/02/06/travel/lithium-ion-batteries/index.html (accessed January 25, 2021).

[57] Tesla's New Autopilot Feature Raises Serious Safety Concerns, Consumer Reports Says, 2019. https://edition.cnn.com/2019/05/22/business/consumer-reports-tesla-navigate-auto-pilot/index.html (accessed January 25, 2021).

[58] A.C. Forse, C. Merlet, J.M. Griffin, C.P. Grey, New perspectives on the charging mechanisms of supercapacitors, J. Am. Chem. Soc. 138 (2016) 5731−5744.